Numerical and experimental investigation of saturated granular column collapse in air

ARTICLE IN PRESS

HOSTED BY

ELSEVIER

Available online at www.sciencedirect.com

ScienceDirect

Soils and Foundations xxx (xxxx) xxx

SOILS AND FOUNDATIONS

www.elsevier.com/locate/sandf

Numerical and experimental investigation of saturated granular column collapse in air

Francesca Ceccato [a,*], Alessandro Leonardi [b], Veronica Girardi [a], Paolo Simonini [a], Marina Pirulli [b]

[a] University of Padua, Department of Civil, Environmental and Architectural Engineering, Via Ognissanti 39, Padua, Italy
[b] Politecnico di Torino, Department of Structural, Geotechnical, and Building Engineering, Corso Duca degli Abruzzi 24, Turin, Italy

Received 25 July 2019; received in revised form 7 April 2020; accepted 18 April 2020

Abstract

Many hazardous natural phenomena like debris flows, avalanches and submerged landslides are governed by the interactions between solid grains and interstitial fluid. They display a complex interplay of physical mechanisms, which are still very challenging to simulate with numerical methods. Different methods have been proposed in the literature to achieve this goal. This paper compares the results of two different numerical approaches: (i) a macromechanical continuum approach with the two-phase double-point Material Point Method (MPM) and (ii) a micromechanical approach with Discrete Element Method coupled with the Lattice Boltzmann Method (DEM-LBM). With the objective of highlighting potentialities and critical points of the two approaches, we conduct saturated granular column collapses in a small-scale laboratory experiment, subsequently reproduced by the numerical codes. Unlike previous experiments of collapse under gravity in dry or completely submerged conditions, in this paper the saturated material is released in air. These conditions better reproduce real natural onshore landslides and allows a discussion on the solid–fluid interaction.

Keywords: 2-phase double-point MPM; DEM-LBM; Column collapse; Soil-fluid interaction

1. Introduction

Many hazardous natural phenomena are characterized by rapid movements of a mixture of solid particles and fluids, and can be defined as flow-like landslides (Hungr et al., 2014). Examples are debris flows, avalanches, and submerged landslides. The study of these phenomena is important for hydro-geological risk assessment and it has attracted the interest of researchers for many years. Fast flow-like landslides exhibit a wide variety of behaviors, which are apparent at a multitude of relevant scales, thus determining a staggering level of complexity (Delannay et al., 2017). Due to these problems, a full understanding of these processes has not been achieved yet.

A commonly employed small-scale model for the study of flow-like landslides is the column collapse (Fig. 1).

Several numerical approaches have been applied to simulate column collapse. They can be conceptually divided into: (*a*) discrete approach such as the Discrete Element Method (DEM), in which the granular material is represented by an assembly of particles interacting at contact points, and (*b*) continuum approach, in which the material is modelled assuming the validity of continuum mechanics theory.

In DEM, the macroscopic behavior of the mass directly derives from micromechanical parameters (contact law, grain characteristics) and state parameters (fabric and

Peer review under responsibility of The Japanese Geotechnical Society.
* Corresponding author.
E-mail address: francesca.ceccato@dicea.unipd.it (F. Ceccato).

https://doi.org/10.1016/j.sandf.2020.04.004

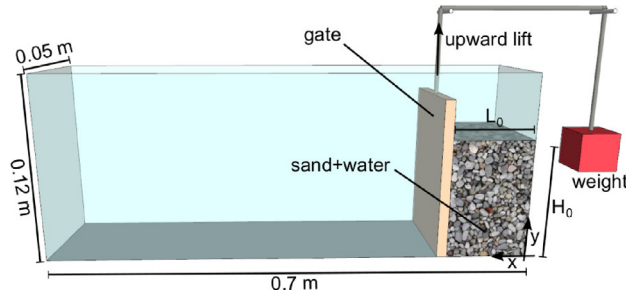

Fig. 1. Illustration of the experimental setup used for column-collapse tests.

porosity). They naturally account for the dependence of the material response to packing and to strain rate (Sun et al., 2013), and can simulate segregation effects (Hill and Tan, 2014). However, the definition of the most appropriate contact model between particles is both a conceptual problem and a source of computational issues. Due to the high computational cost, their use for real-scale events requires careful application of scaling procedures.

The interaction between solid skeleton and interstitial liquid involves the coupling with a fluid solver. The fluid is commonly modelled using simple rheological laws, and solved using a computational mesh. Popular solvers are those stemming from Computational Fluid Dynamics, (CFD-DEM, as in Li and Zhao, 2018) or the Lattice Boltzmann Method (DEM-LBM, as in Švec et al., 2012). With respect to dry DEM, these methods have superior capabilities to describe mixtures, because the dynamics of the ambient fluid is solved. However, they essentially suffer from the same limitations of computational efficiency that affect dry DEM.

Continuum methods, on the other hand, require the definition of a constitutive model to reproduce the stress–strain behaviour of the material. This is one of the major issues of continuum models and the debate around the most appropriate constitutive equation for describing geophysical flows is still active. For example, Fern and Soga (2016) used Mohr–Coulomb and Nor-Sand models to simulate column collapse tests showing that the constitutive model influences the slip surface onset and energy dissipation. Mast et al. (2014) compared a Drucker-Prager model and a hardening–softening Matsuoka-Nakai model showing that the choice of the constitutive model influences the final deposition profile. Ceccato and Simonini (2016) carried out simulations of granular flow impacting a rigid barrier using an elastic perfectly plastic model with Mohr–Coulomb failure criterion, and a viscoplastic model with Drucker-Prager yielding condition, discussing the effect of material parameters.

A continuum approach requires a solver able to accurately manage the large displacements that characterize fast landslides. The last couple of decades has seen a growing use of continuum-based numerical methods to simulate flow-like landslides, which has been tested on column collapse examples. Among these are the Finite Volume Methods (FVM, as in Pirulli et al., 2007; Lagrée et al., 2011), Arbitrary Lagrangian Eulerian Finite Elements (ALE, as in Crosta et al., 2003), the Material Point Method (MPM, as in Fern and Soga, 2016; Solowski and Sloan, 2013; Mast et al., 2014), Lattice Boltzmann Method (LBM, Leonardi et al., 2015b), Particle Finite Element Methods (PFEM, Zhang et al., 2015), and Smoothed Particle Hydrodynamics (SPH, e.g. Dai et al., 2017). These differ greatly in the mathematical description of the process and the discretization of the continuum domain. The general advantage of continuum methods is that they are well suited to real scale events, as they do not suffer from drops in computational efficiency when small particles or large domains are modelled, as occurs in DEM.

In this work, comparison and evaluation of two different numerical methods are carried out (see Section 3): a mixed continuum-discrete DEM-LBM formulation from an in-house code (Leonardi et al., 2015a), and a two-phase double-point Material Point Method (2P-DP MPM) (Bandara and Soga, 2015), recently implemented in the software Anura3D (Martinelli, 2016, www.anura3d.com, 2019). With the objective of highlighting potentialities and critical points of the two approaches, we simulated saturated granular column collapses in air (Fig. 1). Similar uses of DEM-LBM can be found in Kumar et al. (2017) and Yang et al. (2019). However, these applications consider submerged conditions, while this paper accounts for the free surface at the interface between liquid and air.

In Section 5, the numerical results are discussed with emphasis on the collapse dynamics, the run-out, and size scale effects. Moreover, they are compared with small-scale laboratory experiments carried out at the University of Padua. Unlike previous experiments of column collapse in completely submerged conditions, completely dry conditions or with a very small amount of fluid (see e.g. Lube et al., 2005; Artoni et al., 2013; Bougouin and Lacaze, 2018; Santomaso et al., 2018; Jing et al., 2018, among others), the material is saturated and propagates in air (see Section 2 for more details). These conditions are closer to natural flow-like landslides.

2. Experimental tests

The experimental configuration is illustrated in Fig. 1. It consists in a standard glass flume 0.70 m-long, 0.05 m-wide, and 0.12 m-high, closed at one end. The flume is equipped with a movable vertical gate at a distance of $L_0 = 0.04$ m from the closed end: in this way, a storage partition is created, where the saturated granular mixture is placed. By modifying the filling height, columns with different aspect ratios can be prepared. The channel base and the lateral walls are made of glass, while the gate is made of plexiglass. The gate and the opening mechanism have been designed to address both water-tightness before collapse and sudden gate uplift. The first is crucial to avoid partial desaturation prior to the collapse, thus an immiscible fluid (vaseline) was used to coat the interfaces between gate and

Please cite this article as: F. Ceccato, A. Leonardi, V. Girardi et al., Numerical and experimental investigation of saturated granular column collapse in air, Soils and Foundations, https://doi.org/10.1016/j.sandf.2020.04.004

flume sides; in addition, the same fluid favors the fast uplift of the gate, triggering the propagation of the saturated mixture in a way that can be well described by the sudden removal of fixities in the numerical models.

The granular material has a uniform granulometric distribution with mean diameter $D = 2.5 \cdot 10^{-3}$ m and grain density $\rho_S = 2625\ \mathrm{kg/m^3}$. The fluid phase is water dyed with a natural colorant to improve the visualization of the fluid motion.

The preparation method of the saturated sample aims at controlling the initial volumetric fractions of the components. At the beginning, the column volume is filled with $2 \cdot 10^{-5}\ \mathrm{m^3}$ of water. Subsequently, a controlled amount of granular material is gently poured with a spoon immersed in the water to allow deposition without compaction and to avoid gas bubble inclusion. Soil layering continues until the column reaches the desired initial dimensions. If necessary, the water level is adjusted using a syringe. The liquid volume V_L and the solid mass m_s are carefully measured; the porosity is computed from the liquid volume as $n_{V_L} = V_L/(H_0 L_0 W)$, and subsequently cross-checked with a second equation based on solid mass: $n_{m_s} = 1 - m_s/(\rho_s H_0 L_0 W)$. Some differences were reported in the initial aggregation state due to the operator influence on the preparation procedure, in fact the initial porosity values were always bounded between 0.39 and 0.43, with an average of 0.40.

The experimental tests considered in this paper are summarized in Table 1. The initial column basal dimensions are fixed, since they are related to the apparatus configuration, while the height of the column is varied between $H_0 = 0.03$ m and 0.07 m, obtaining different aspect ratios $a = H_0/L_0$. Three tests for each configuration are carried out to verify the repeatability of the results and estimate the experimental error.

The apparatus is illuminated by a constant artificial led light. The process is recorded with a high-resolution and high-speed camera (500 frames/s) placed at the channel side, and aligned to the horizontal channel axis. Separate frames are extracted from the video and the edges of the column are detected extracting the corresponding coordinates data set with an in-house MatLab code (Brezzi, 2018). Note that with this procedure only the lateral profile of the column can be observed.

Fig. 2 provides an overview of the collapse evolution for $a = 1.5$, with four extracted frames overlapping with the detected profiles (in red). Time is normalized with respect to a reference time, defined in accordance with previous numerical studies on dry and submerged granular column collapse: $t_{\mathrm{ref}} = \sqrt{H_0/g}$ for dry conditions and $t_{\mathrm{ref}} = \sqrt{H_0/g\prime}$ for saturated conditions. The reduced gravity $g\prime = g(\rho_S - \rho_L)/\rho_S$ accounts for the buoyancy effect in the ambient fluid (Meruane et al., 2010; Jing et al., 2018).

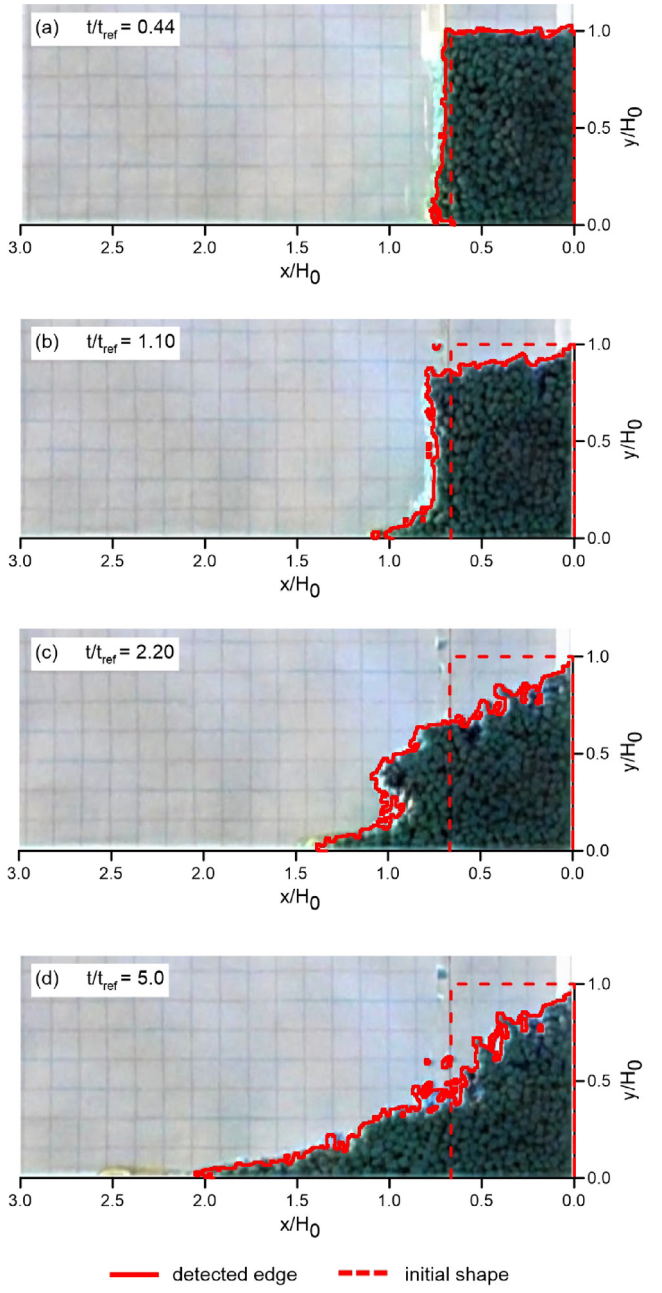

Fig. 2. Frames of the saturated soil collapse experiment ($a = 1.5$) with edge detection at different time instants.

When the gate is lifted, at the toe of the column both grains and water start moving forward (Fig. 2a). Then, the top part heads toward the flume base, slipping along a failure surface progressively evolving with time (Fig. 2b, c). Finally, the granular front decelerates and stops, while water filters through the solid phase (Fig. 2d).

Table 1
Summary of experimental tests. The aspect ratio is computed as $a = H_0/L_0$.

Conditions	H_0 [m]	L_0 [m]	a [–]	Grain number
Saturated and Dry	0.07	0.04	1.75	≈ 9300
	0.06	0.04	1.50	≈ 8000
	0.05	0.04	1.25	≈ 6700
	0.04	0.04	1.00	≈ 5300
	0.03	0.04	0.75	≈ 4000

Please cite this article as: F. Ceccato, A. Leonardi, V. Girardi et al., Numerical and experimental investigation of saturated granular column collapse in air, Soils and Foundations, https://doi.org/10.1016/j.sandf.2020.04.004

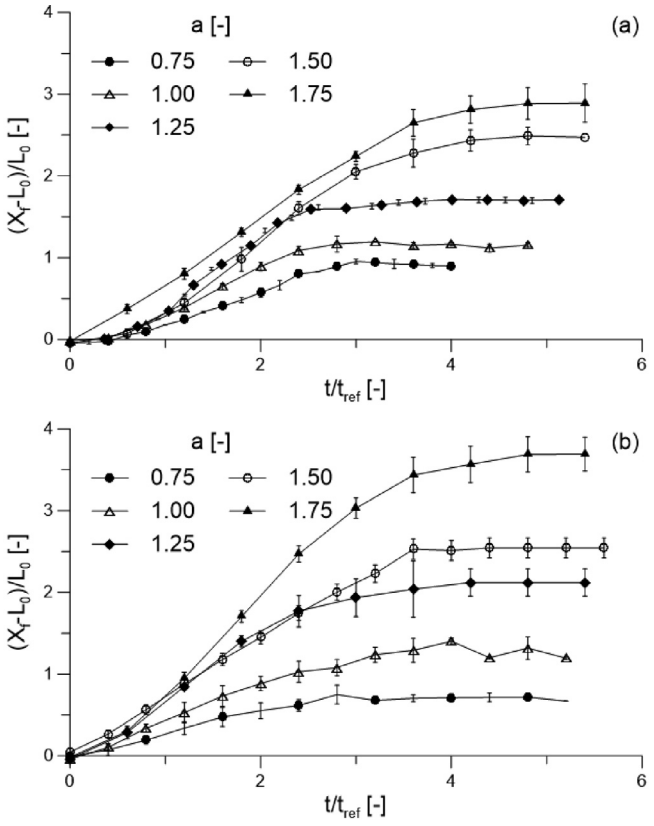

Fig. 3. Time evolution of normalized front position for dry (*a*) and saturated cases (*b*).

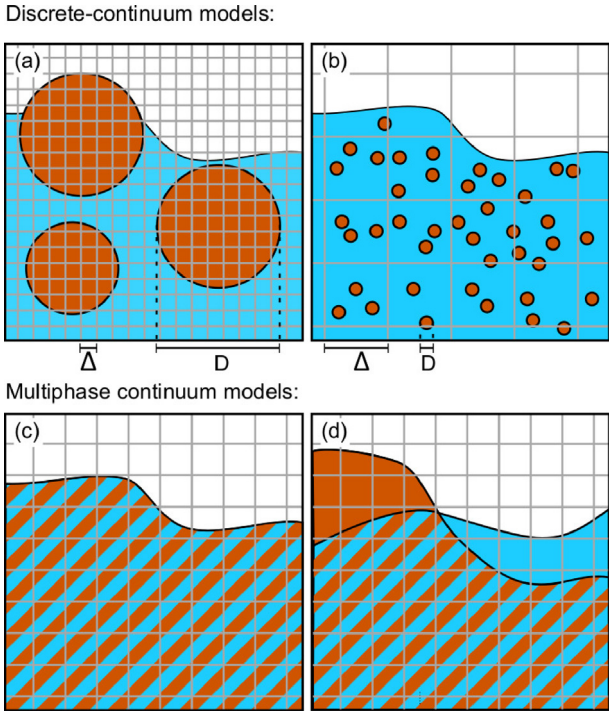

Fig. 4. Comparison between (*a*) continuum-discrete coupling strategies where the drag force is computed through integration (typical of DEM-LBM and used in this work), (*b*) continuum-discrete coupling based on an analytical drag formulation (typical of DEM-CFD), (*c*) continuum methods employing a single-phase mixture, (*d*) continuum methods representing independent interacting phases, as the 2P-DP MPM model employed here.

Fig. 3 plots the evolution of the normalized front position $(X_f - L_0)/L_0$ as function of the normalized time t/t_{ref} for different aspect ratios in dry and saturated conditions. The evolution of the process and the runout are very similar in dry and saturated conditions for $a \leqslant 1.0$. In contrast, the process is slightly faster in terms of normalized time and the runout is longer in saturated conditions for $a > 1.0$.

3. Outline of the numerical methods

This section presents the numerical methods applied in this study and discusses the differences and similarities with other approaches.

In order to apply DEM to saturated media, it is coupled with a fluid solver. Two main approaches can be used: (a) a fluid mesh size Δ smaller than the characteristic particle diameter D (Fig. 4a), in this way the interpore fluid pressure field is solved accurately and the calculation of the solid–fluid interaction force is carried out by direct integration; and (b) a fluid mesh size larger than the characteristic particle diameter $\Delta \gg D$ (Fig. 4b), which requires to estimate the interaction force with an analytical equation based on a value of fluid velocity interpolated from the neighbouring cells. The first strategy is commonly applied in DEM-LBM, while the second is typically adopted by CFD-DEM. However, there exist CFD-DEM applications that compute drag through integration (Leonardi et al., 2018), and DEM-LBM models that rely on interpolation (Xiong et al., 2014).

The main differences among continuum-based numerical approaches applied for saturated media lie in the assumptions used to derive the governing equations of the process and in the discretization strategy. From the mathematical point of view, the governing equations of motion can be derived assuming that the solid–fluid mixture behaves as an equivalent one-phase medium, as illustrated in Fig. 4 (*c*). Alternatively, the balance equations of each phase can be solved separately. The latter is more advanced, and in some methods complete separation between the phases can be achieved, as shown in Fig. 4 (*d*). The 2P-DP MPM uses this approach (Abe et al., 2013; Bandara and Soga, 2015; Martinelli and Rohe, 2015). From the numerical point of view the continuum equations can be discretized using a grid (mesh-based methods), as in FVM, ALE, LBM, or computational points (particle-based methods), called material points (MPs) or particles, as in MPM, PFEM, SPH.

3.1. DEM-LBM

DEM-LBM is a hybrid approach where two different simulation strategies are employed for the two phases,

Please cite this article as: F. Ceccato, A. Leonardi, V. Girardi et al., Numerical and experimental investigation of saturated granular column collapse in air, Soils and Foundations, https://doi.org/10.1016/j.sandf.2020.04.004

and a coupling algorithm tracks the inter-phase transmission of forces.

The granular phase is simulated with DEM as a collection of spherical particles which interact through binary collisions. The particles contacts are resolved by allowing a small overlap ξ, which determines a repulsive force normal to the contact surface. This is equal, in magnitude, to

$$F_n = k_n \xi + \alpha_n \sqrt{k_n m} \frac{d\xi}{dt}, \quad (1)$$

with k_n and α_n the normal contact stiffness and damping, respectively, and m the particle mass. In the tangential direction, an analogous force is exchanged, whose magnitude is modulated by a friction coefficient μ_s, and is equal to

$$F_t = \max\left(\mu_s F_n, k_t \zeta + \alpha_t \sqrt{k_t m} \frac{d\zeta}{dt}\right), \quad (2)$$

where ζ is the length of a spring connecting the initial contacts points on the two particle surfaces, and $k_t = 2/7 k_n$ and α_t the tangential contact stiffness and damping. Additionally, a rolling resistance has been implemented in order to reduce the spurious effects due to the use of spherical particles. It consists of an additional torque M_r, which opposes to relative rolling between particles. Its magnitude is proportional to the normal contact load:

$$M_r = \mu_r F_n \frac{D}{2}, \quad (3)$$

where μ_r is a coefficient of rolling friction, analogous to μ_s. Note that in case particles with different diameters collide, effective values for the mass and the diameter should be used instead of m and D. More details about the contact model can be found in Marchelli et al. (2019).

The particles are immersed in a fluid phase, whose dynamics is solved with LBM. The fluid mesh size is smaller than the characteristic diameter of the particles, i.e. $\Delta < D$, Fig. 4 (*a*). This implies that the pore pressure is effectively resolved, and that the drag force can be computed by integration of singular drag contributions coming from all fluid cell interacting with each particle (Leonardi et al., 2015a). The free surface position is updated using a volume-of-fluid method (Janßen and Krafczyk, 2011).

In LBM, field variables such as macroscopical fluid velocity $\mathbf{v}_L$ and density ρ_L are recovered by tracking the state of a distribution function, which is discretized in space on a regular lattice with spacing Δ, time t, and microscopical velocity. The latter is performed by selecting a small set of discrete microscopical velocities. The lattice model used here works with 19 discrete velocities in 3 dimensions, and is known as D3Q19.

Following Feng et al. (2010), a Smagorinsky turbulence model is implemented, with a turbulent viscosity ν_t, proportional to the shear rate, added to the molecular viscosity of water ν_m:

$$\nu = \nu_m + \nu_t = \nu_m + (C\Delta)^2 \dot{\gamma}, \quad (4)$$

where C is the Smagorisnky constant, here assumed constant and equal to 0.16, and $\dot{\gamma}$ is the second invariant of the shear-rate tensor.

A key aspect of DEM-LBM, as already mentioned, is that the DEM particle diameter D is required to be larger than the lattice spacing Δ (Fig. 4 (*a*)). Therefore, multiple fluid cells are located within each DEM particle. These cells exchange a drag force $\mathbf{f}_d$ with the particles, determined with a direct-forcing immersed-boundary method (Švec et al., 2012), as:

$$\mathbf{f}_d = \Delta^3 \rho_L (\mathbf{v}_L - \mathbf{v}_P), \quad (5)$$

where Δ^3 is the volume of the fluid cell, and $\mathbf{v}_P$ the particle velocity.

The integration in time is explicit for both DEM and LBM, but the time-step required by DEM is usually smaller than the one required by LBM. The two solvers are thus called in a staggered fashion, with multiple DEM iterations in between two consecutive LBM steps. More details about the method, its limitations, and possible applications can be found in Leonardi et al. (2015a).

3.2. Two-phase double-point MPM

The 2P-DP formulation for MPM was initially presented by Abe et al. (2013), and later extended by Bandara and Soga (2015) and Martinelli and Rohe (2015). In this section the key features of the model are briefly summarized. The reader should refer to Fern et al. (2019) and references therein for further details.

The formulation assumes that the soil is a superposition of two continuum media: the solid skeleton and the liquid phase. These are represented separately by two sets of Lagrangian MPs: solid material points (SMPs) and liquid material points (LMPs). The computational domain in which the material moves is discretized with a finite element mesh. According to this framework, three possible domains can emerge (Fig. 4 *d*):

- Porous medium in saturated conditions, when SMPs and LMPs share the same grid element;
- Porous medium in dry conditions, when only SMPs are located in the grid element;
- Free liquid, when only LMPs are located in the grid element.

The dynamic behaviour of the continuum is described with the solid and liquid dynamic momentum balances, which are solved at the grid nodes. The mass balance of the solid phase, the liquid, and the mixture are posed at the corresponding MPs in order to update secondary variables. The same operation is performed for the constitutive relationships. The software applies an explicit time integration scheme. The force representing the interaction between solid and fluid, $\mathbf{f}_{SL}$, assumes the expression proposed by Vardoulakis (2004) (Eq. (6))

Please cite this article as: F. Ceccato, A. Leonardi, V. Girardi et al., Numerical and experimental investigation of saturated granular column collapse in air, Soils and Foundations, https://doi.org/10.1016/j.sandf.2020.04.004

$$\mathbf{f}_{SL} = \mathbf{f}_n + \mathbf{f}_d = \boldsymbol{\sigma}_L \nabla n_L + \mathbf{f}_d. \quad (6)$$

In this expression, $\mathbf{f}_n$ accounts for the porosity gradient. This term is not necessary in DEM-LBM, where the pore space is resolved. The second term, $\mathbf{f}_d$, is a drag force, a function of the relative velocity between fluid and solid ($\mathbf{v}_L - \mathbf{v}_S$), which finds an equivalent on DEM-LBM in Eq. (5). In Eq. (6), n_L is the liquid volumetric fraction, which coincides with porosity in saturated media, and $\boldsymbol{\sigma}_L$ is the stress tensor of the liquid phase.

The drag law proposed by Forchheimer (1901) is implemented in the 2P-DP formulation:

$$\mathbf{f_d} = \mathbf{f_1} + \mathbf{f_2} = \frac{v}{k_L} n_L^2 (\mathbf{v_L} - \mathbf{v_S}) + \beta n_L^3 \rho_l |\mathbf{v_L} - \mathbf{v_S}| (\mathbf{v_L} - \mathbf{v_S}). \quad (7)$$

It includes a linear term $\mathbf{f}_1$ (low-velocity regime) and a quadratic term $\mathbf{f}_2$ (high velocity regime). The former is a Stokesian drag term, employed in a similar form also in DEM-LBM (Eq. (5)). The latter, named the non-Darcy flow coefficient, has been estimated by many authors both numerically and experimentally. It shows dependence on porous media features like permeability, porosity and tortuosity (Li et al., 2001; Orodu et al., 2012). The formulation applied in this study determines the empirical coefficient β using Ergun coefficients (Eq. (8)) (Ergun, 1952) $A = 150, B = 1.75$.

$$\beta = B / \sqrt{\kappa_L A n_L^3}. \quad (8)$$

The intrinsic permeability κ_L can evolve in time due to the variation of porosity. This is taken into account with a Kozeny-Karman formula (Eq. (9)):

$$\kappa_L = \frac{D^2}{150} n_L^3 / (1 - n_L)^2. \quad (9)$$

Granular materials can experience a transition between solid-like behaviour to fluid-like behaviour when the porosity and the shear rate increase. The 2P-DP formulation accounts for the phase transition process by a maximum porosity criterion. Below a threshold porosity value (n_{max}) solid-like behavior persists (*Solid state*) with positive effective stress, updated with constitutive relations typical of soils, like Mohr–Coulomb.

Conversely, above the maximum porosity, grains are supposed to be detached. Thus, the stress transmission is no more possible, the effective stress is zero and the soil behaves like a fluid (*Liquid state*), with an effective viscosity ν_{eq} (Eq. (10)) (Beenakker, 1984), affected by the solid volumetric fraction $(1 - n_L)$.

$$\nu_{eq} = \nu_m \left(1 + \frac{5}{2}(1 - n_L) + 5.2(1 - n_L)^2\right) \quad (10)$$

In this formulation, the liquid phase is assumed weakly compressible and the stress increment is computed with Eq. (11)

$$\dot{\boldsymbol{\sigma}}_L = p_L \boldsymbol{I} + \dot{\sigma}_{L,dev} = K_L \dot{\varepsilon}_{vol,L} \boldsymbol{I} + 2\nu_{eq} \dot{\boldsymbol{\varepsilon}}_L, \quad (11)$$

where K_L is the liquid bulk modulus, $\boldsymbol{I}$ is the identity vector, $\dot{\boldsymbol{\varepsilon}}_L$ is the liquid strain increment and $\dot{\varepsilon}_{vol,L}$ is its volumetric component.

In elements with SMPs in *Solid state* the deviatoric part of the liquid stress tensor is assumed to be zero ($\dot{\sigma}_{L,dev} = 0$). In *Liquid state*, i.e. as soon as fluidization occurs, the deviatoric component is computed considering Eq. (10) for the equivalent viscosity.

4. Setup and calibration of numerical models

The methods outlined in the previous section are used to reproduce numerically the column collapse tests described in Section 2. The main differences are the type of description employed for the solid phase (discrete in DEM-LBM, continuum in 2D-DP MPM), and the geometrical degree of simplification (3D for DEM-LBM, 2D for 2P-DP MPM). Preliminary 3D numerical analyses with MPM confirmed that the results of the 2D model are not significantly affected by geometrical effects, thus the plane-strain model can be effectively applied to reduce the computational cost. While the fluid material parameters are relatively straightforward to determine, the solid phase parameters are obtained through calibration.

4.1. DEM-LBM model setup

The DEM-LBM model is fully three-dimensional and counts from 4000 to 9300 particles, depending on the column height H_0. Boundary walls have frictional properties when interacting with the solid phase. Following Eq. (2), particles can slip on the surface only when the friction is overcome. Identical frictional coefficients are assumed for the particle–particle contact and for the wall-particle contact. For the fluid phase, the no-slip boundary condition is applied at all boundaries.

The initial sample is assembled by gravity-induced deposition of the particles in dry conditions inside the release tank, and by subsequently filling the pores with liquid. Concerning the liquid phase (LBM), pure water is considered and the molecular viscosity of water is assumed equal to 10^{-3} Pa · s.

LBM is discretized using a uniform grid spacing of $\Delta = 6 \cdot 10^{-4}$ m in each direction. This spacing results in $D/\Delta \simeq 4$, which is sub-optimal with respect to the accuracy of resolution of the pore space. This choice has two major implications. Firstly, the particle shape is only roughly resolved by the fluid solver. This error has limited effects on the simulation accuracy, since the spherical shape is only an approximation of the real particle shape. More importantly, the permeability of the granular medium may be different from the experimental one. This is probably compensated by the slightly looser packing obtained using spheres ($n = 0.42$) with respect to the real grains. In any case, the use of a rougher grid allows to run DEM-LBM simulations in a relatively short time (typically a

Please cite this article as: F. Ceccato, A. Leonardi, V. Girardi et al., Numerical and experimental investigation of saturated granular column collapse in air, Soils and Foundations, https://doi.org/10.1016/j.sandf.2020.04.004

few days), thus limiting the difference in computational cost with respect to the pure-continuum model, which completes the simulation in a few minutes. The time step is uniform and equal to $8 \cdot 10^{-5}$ s. Between two consecutive LBM iterations, 57 DEM time steps are performed.

4.2. 2P-DP MPM model setup

For the pure-continuum strategy, a two-dimensional MPM model is used, in plain strain conditions. Frictional effects of the lateral boundary are neglected, and we assume that they are small at the symmetry plane of the experiment. The bottom boundary is fixed (i.e. fully rough), while roller boundary conditions are applied at the other surfaces. A linear-elastic perfectly-plastic model with a Mohr–Coulomb failure criterion is used.

The MPM model applies a structured mesh with element size of $4 \cdot 10^{-3}$ m; 12 LMPs and 12 SMPs are assigned to each initially active element. A small value of local damping (0.02) is used to stabilize the results (Ceccato and Simonini, 2019). This small damping coefficient does not influence significantly the runout. The influence of element size, MPs number, and local damping has been deeply discussed in previous works (Fern and Soga, 2016) considering dry column collapse simulated with a one-phase approach. It was shown that mesh refinement improves the definition of the failure surface, while having a small effect on the runout. These considerations are confirmed for the 2P-DP MPM model considered in this study. However, while in the dry case increasing the number of MPs does not improve significantly the results, with the 2P-DP approach, the use of only 3 MPs/elem sometimes leads to numerical instabilities, and better results are obtained with 12 MPs/elem. A larger number of MPs reduces the quadrature error (Steffen et al., 2010) and the occurrence of elements filled with only a small number of MPs, which seems to be very important for the stability of 2P-DP MPM. A further increase of the number of MPs increases the computational cost without improving the results.

The boundary conditions for the liquid are identical to those of the solid. A simple Newtonian model is used to describe the material. In the 2P-DP MPM model, a reduced value of the bulk modulus ($2 \cdot 10^7$ Pa) compared to pure water is used to speed up the calculation. A cavitation threshold is imposed in MPM to overcome numerical difficulties, thus only positive pressures are allowed.

As with LBM, the method has been extensively tested in the classical one-phase dam-break problem, showing good agreement with experimental results and other numerical methods (Janßen and Krafczyk, 2011; Zhao et al., 2017).

Following the experimental configuration, a mean diameter of $2.5 \cdot 10^{-3}$ m is used to update the intrinsic permeability and the drag force, with Eq. (7) and Eq. (9). The initial porosity is set to 0.4.

In the MPM model the initial stress state is initialized during a gravity loading step in which gravity is applied while preventing horizontal displacement of both sides of the column. The horizontal fixity on the left boundary is then removed and the failure of the column is initiated.

4.3. Calibration in dry conditions

Before studying saturated conditions, a preliminary calibration of the material parameters governing the behavior of the solid phase is carried out based on dry column collapse tests. A reference height $H_0 = 0.06$ m is considered for calibration.

In DEM, micromechanical parameters are calibrated following Marchelli et al. (2019). In particular, different combinations of friction and rolling coefficients (μ_s in the range $[0.4, 0.8]$, and μ_r in the range $[0.01, 0.15]$) are tested, while keeping a constant restitution coefficient. The final set of parameters is selected by comparing the final deposit shape in numerics and experiments. The particle contact stiffness k_n does not correspond to the physical value, which would result in prohibitively small DEM time steps. However, it is sufficiently high to keep the system within the rigid limit, as defined by Roux and Combe (2002). In this state, a change in stiffness does not alter significantly the system kinematics.

In MPM, a series of parametric analyses has been performed to calibrate the macroscopic friction angle showing that $\phi = 35°$ gives the best results.

Table 2 lists the chosen set of parameters for both DEM and MPM models. The simulation results that give the best fit with the experimental data are illustrated in Fig. 5.

5. Numerical results in saturated conditions

The current section presents the numerical results obtained in saturated conditions for the cases summarized in Table 1. A cross-comparison between 2P-DP MPM and DEM-LBM is performed.

5.1. Collapse dynamics

In the experiments, after gate opening, the granular material collapses and water tends to flow out of the sample. At the same time, the top part of the column desaturates. When the granular material mobilizes, the grains closer to the free boundary accelerate and the number of contacts decreases, with the superficial layer of material moving towards fluidized conditions.

The evolution of the granular fabric can be well visualized with the DEM. In the discrete simulations, the mean coordination number (i.e. the mean number of contacts per particle) is initially relatively high, and decreases during the acceleration (see Fig. 6). This is particularly prominent in the shallow part of the column. The mean coordination number increases again during deposition. Fig. 7 shows how the percentage of grains with a high coordination number, e.g. 4, 5 or 6, decreases during motion. A sharp rise in disconnected particles (zero coordination number)

Please cite this article as: F. Ceccato, A. Leonardi, V. Girardi et al., Numerical and experimental investigation of saturated granular column collapse in air, Soils and Foundations, https://doi.org/10.1016/j.sandf.2020.04.004

Table 2
Material parameters used for the DEM and MPM simulations.

DEM		MPM	
Grain density ρ_S [kg/m^3]	2600	Grain density ρ_S [kg/m^3]	2600
Norm. cont. stiffness k_n [N/m]	$0.2 \cdot 10^4$	Initial porosity n [–]	0.4
Tan. cont. stiffness k_t [N/m]	$0.057 \cdot 10^4$	Poisson ratio [–]	0.3
Damping $\alpha_{n(t)}$ [–]	0.04	Young Modulus [Pa]	10^7
Restitution coef. [–]	0.88	Cohesion [Pa]	0.0
Friction coef. μ_s [–]	0.577	Friction angle [°]	35
Rolling coef. μ_r [–]	0.05		

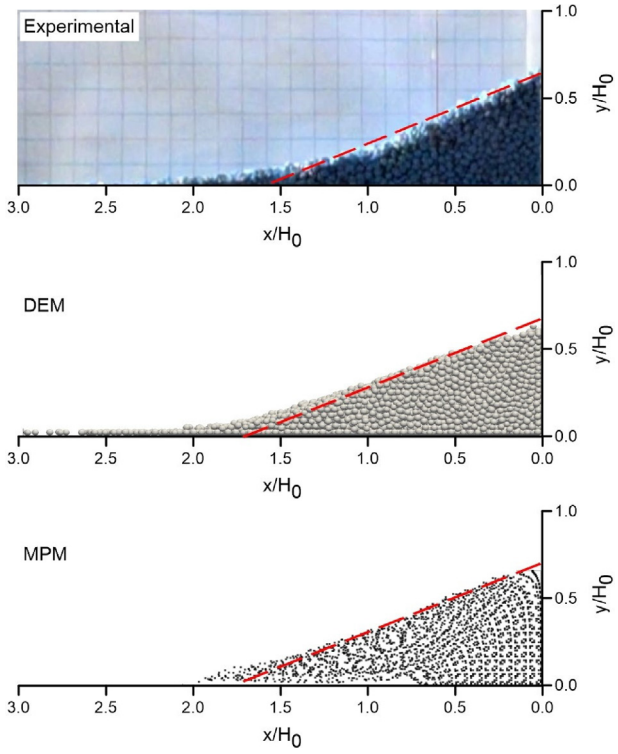

Fig. 5. Final configuration of dry column collapse: experimental vs. numerical results.

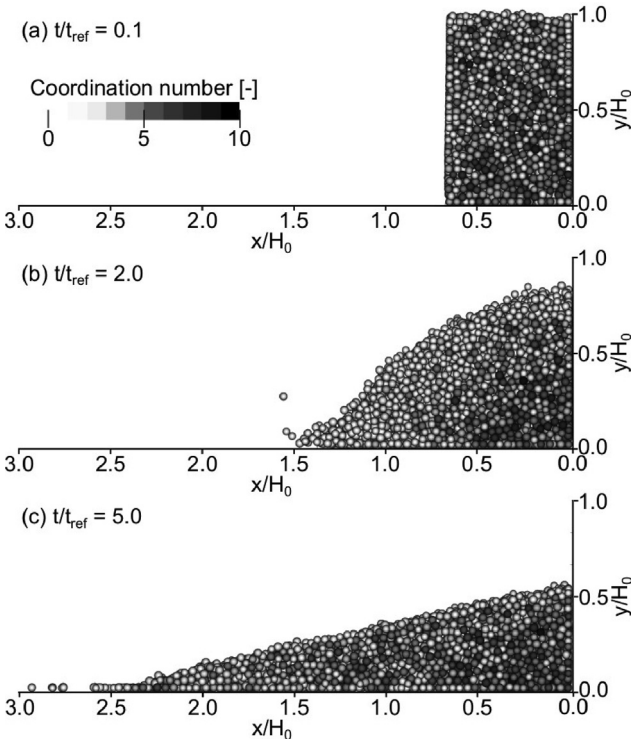

Fig. 6. Statistical distribution of the coordination number at different time instants.

is observed from $t/t_{ref} = 0.1$ to 2. At the same time, the percentage of grains with a higher coordination number lowers. At the beginning of the simulation, and at deposition, the column approaches static conditions; notwithstanding the differences in the macroscopic shape of the mass, the distribution of the coordination number is similar in these two states.

Conversely, in the pure continuum model the granular microstructure is not resolved, and no information on the coordination number is available. The change of state in the medium can nevertheless be observed. It appears as a decrease of the mean effective stress due to the lack of confinement at the top and lateral boundaries of the column. At these locations, the effective porosity increases, bringing (eventually) the solid to the fluidized state. In this state, soil effective stress is zero, and its presence in the fluid phase increases the apparent viscosity, according to Eq. (10). The boundary between fluidized and non-fluidized state is

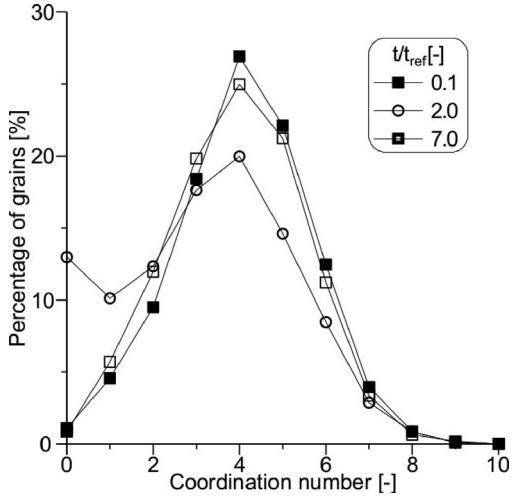

Fig. 7. Percentage of grains with a specific coordination number at different time instants.

Please cite this article as: F. Ceccato, A. Leonardi, V. Girardi et al., Numerical and experimental investigation of saturated granular column collapse in air, Soils and Foundations, https://doi.org/10.1016/j.sandf.2020.04.004

n_{max}, which is a model parameter. Fig. 8 shows the phase status at SMPs at $t/t_{ref} = 2$ for $n_{max} = 0.5$ and $n_{max} = 0.8$. This parameter affects the soil profile slightly, but does not seem to be relevant for the runout and the collapse dynamics.

Fig. 9 compares the results obtained with the two numerical models for the case $H_0 = 0.06$ m. The MPM model (panels *a-c*) predicts a faster collapse, with higher front velocity and no clear separation between granular and liquid fronts. In the DEM-LBM model (panels *d-f*), the collapse develops more slowly and the formation of a granular front is recognizable up to $t/t_{ref} = 5$. After this time, the water slowly flows out of the soil.

As an example, for the cases $H_0 = 0.03$ m, 0.05 m, and 0.07 m ($a = 0.75, 1.25$, and 1.75, respectively) the time-evolution of the normalized solid front position is shown in Fig. 10 comparing numerical and experimental results. The position of the front in the numerical simulations is defined as the horizontal coordinate $X_{f,S}$ overtaken by 0.5% of the total solid mass.

The evolution of the front position simulated by DEM-LBM is slightly slower than the 2P-DP MPM and the experimental results, especially for $a = 1.75$.

The difference in collapse speed can be explained as due to three simultaneous effects. Firstly, DEM-LBM is more dissipative, because it resolves the energy losses due to granular collisions. These are not directly considered in the Mohr–Coulomb model applied in 2P-DP MPM

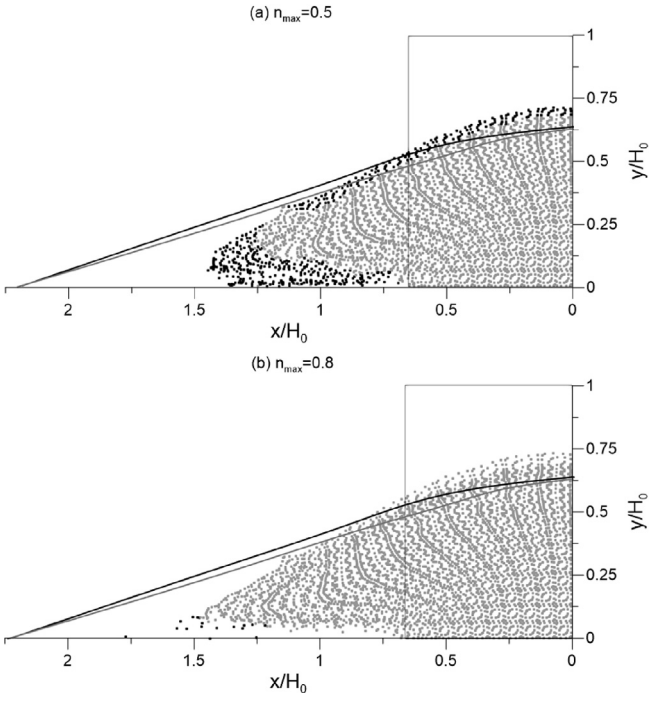

Fig. 8. Phase status of SMPs at $t/t_{ref} = 2$ in case (*a*) $n_{max} = 0.5$ and (*b*) $n_{max} = 0.8$. Black points are in fluidized state, grey points are in solid state. The grey and black lines indicate the final deposition for $n_{max} = 0.5$ and $n_{max} = 0.8$ respectively.

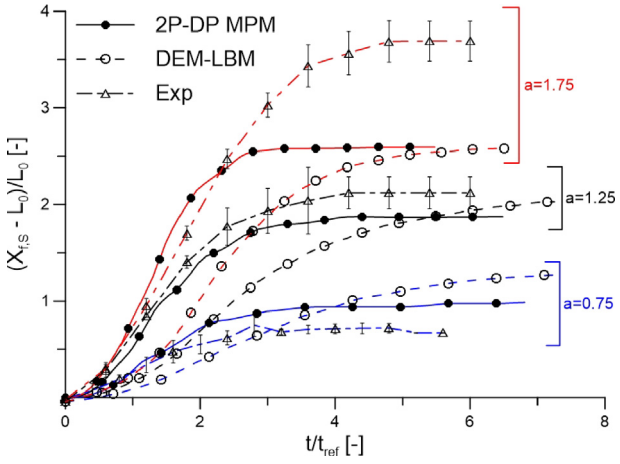

Fig. 10. Evolution of normalized front position in time for different aspect ratios. Numerical results (hollow circles for DEM-LBM and full circles for 2P-DP MPM) and experimental results (triangles) in saturated conditions.

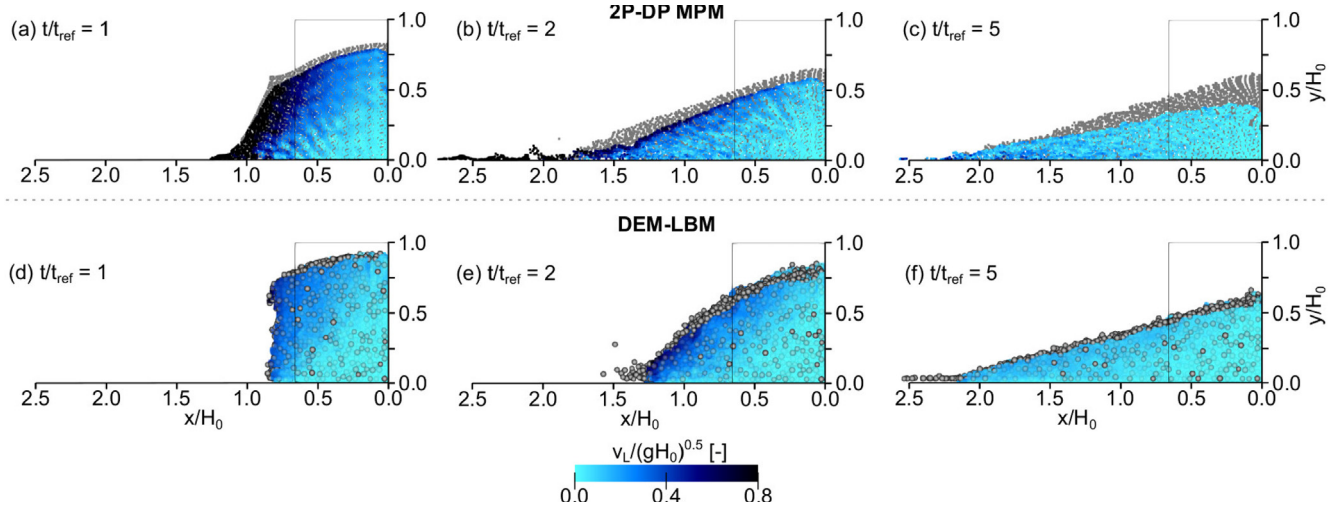

Fig. 9. Numerical results at three time instants $t/t_{ref} = 1; 2; 5$. Grey circles indicate the position of the solid phase (SMPs or DEM particles) while a colour scale is used to visualize the normalized fluid speed $v_L/(g(H_0)^{0.5}$.

Please cite this article as: F. Ceccato, A. Leonardi, V. Girardi et al., Numerical and experimental investigation of saturated granular column collapse in air, Soils and Foundations, https://doi.org/10.1016/j.sandf.2020.04.004

(Redaelli et al., 2017b). Second, DEM-LBM can account for negative pore pressures when the granular skeleton dilates. Conversely, in the 2P-DP MPM formulation the excess pore pressure can only be positive due to numerical difficulties. Thus, in the pure-continuum model the changes in pore pressure can promote granular mobility, but cannot reduce it. Since granular columns in loose packing are considered here, this effect must be limited. Third, DEM-LBM considers the confining effect of the lateral walls, but this is minor compared to other contributes.

After the initial collapse stage, DEM-LBM exhibits a continuous flow of fluid out of the deposit body. In the experiment, this is not observed, due to the retaining effect of surface tension, which is not included in our numerical formulations. Thus, the flow front in DEM-LBM does not reach static conditions for the fluid phase until the totality of the fluid has filtered out of the granular deposit. This process happens on a timescale that is much longer than t_{ref}, but nevertheless has the effect of increasing the measured runout for the DEM-LBM simulations.

From direct observation, the fluid front appears to be slightly ahead of the granular front in all tests. MPM correctly reproduces this behavior, see Fig. 10. In DEM-LBM though, the granular front is almost always faster. This could be due to the resolution of the pore space in DEM-LBM, as mentioned already in Section 4.1. Especially when the grains are agitated, as is the case within the granular front, this can cause an apparent reduction of permeability. On the other hand, DEM-LBM is able to reproduce very realistically the detachment of particles from the main body, which is very difficult to reproduce in MPM due to the continuum assumption.

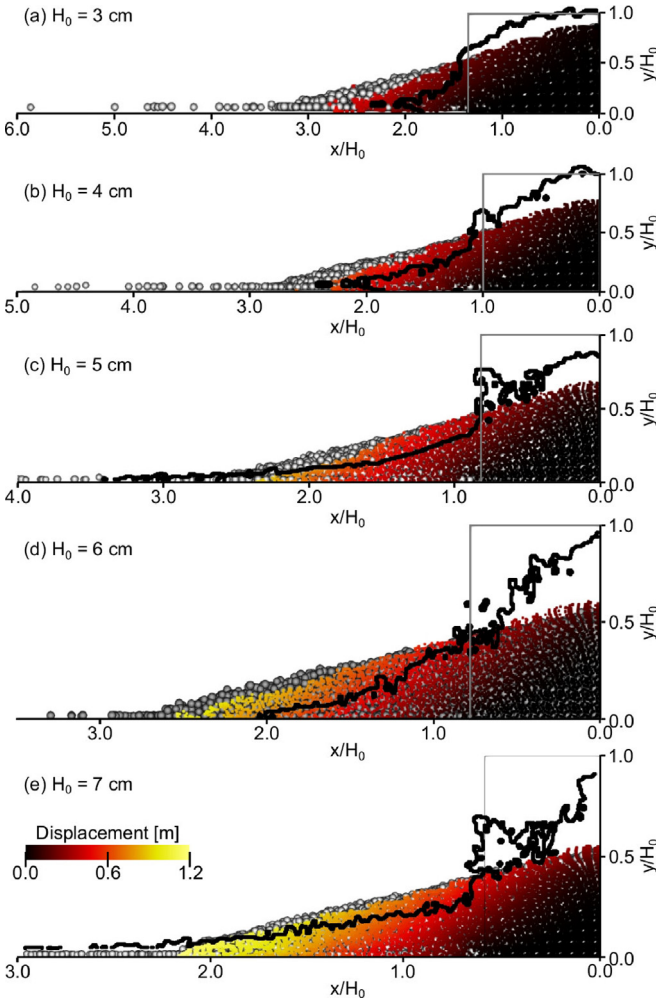

Fig. 11. Final configuration of the saturated column collapses for $H_0 = 0.03, 0.04, 0.05, 0.06, 0.07$ m (red or yellow dots stands for SMPs, grey spheres are DEM solid grains and the black line is the experimental profile).

5.2. Deposition

Fig. 11 shows the final shape of the deposit for different initial column heights obtained with MPM (red-yellow dots) and DEM-LBM (grey circles). The black line indicates the experimental profile. The final shape of the solid deposit in MPM is approximately a straight line, while in DEM-LBM it is convex. This effect is due to the discrete description of the granular assembly in DEM-LBM. There is a relatively good agreement between the two numerical models.

The discrepancies with the experimental results are mainly due to the behavior of the top part of the column. This is in partially saturated conditions, and not completely dry as assumed by the numerical models. In the experiments, some grains and fluid remain attached to the lateral walls due to the fluid surface tension. These are recognized by the edge detection algorithm. This effect is pronounced only within the area covered by the initial position of the column, which is shown in Fig. 11 with a hollow rectangle. Outside of this area, the surface detection is fair.

The normalized runout $(L_f - L_0)/L_0$ as a function of the aspect ratio is plotted in Fig. 12. The results obtained in this study for the saturated column (sat) simulated with DEM-LBM and 2P-DP MPM are compared with the experimental results in dry and saturated conditions and with literature studies by Bougouin and Lacaze (2018) and Jing et al. (2018). Bougouin and Lacaze (2018) carried out laboratory experiments in fully submerged conditions (sub) with different ambient fluid and particle diameter. Jing et al. (2018) simulated dry and submerged column collapse tests with CFD-DEM. The results of the present study consider saturated column collapse in air, thus the differences with literature results could be due to the presence of the ambient fluid. Both numerical models slightly overestimate the runout for $a = 0.75$, but there is a relatively good agreement in the other considered cases.

5.3. Considerations on the drag force

In multiphase continuum methods the definition of the drag force is an essential ingredient of the model. The ratio between the quadratic and the linear term in Eq. (7) is pro-

Please cite this article as: F. Ceccato, A. Leonardi, V. Girardi et al., Numerical and experimental investigation of saturated granular column collapse in air, Soils and Foundations, https://doi.org/10.1016/j.sandf.2020.04.004

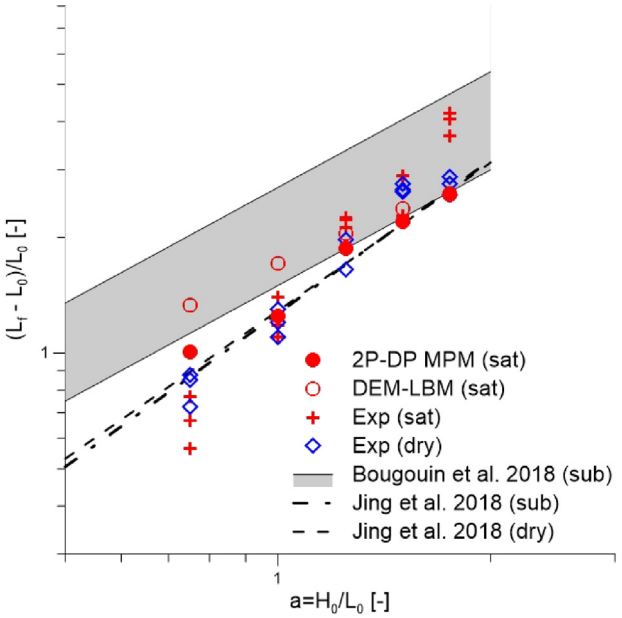

Fig. 12. Normalized runout as function of the initial aspect ratio a, *dry* = dry column collapse in air, *sat* = saturated column collapse in air, *sub* = submerged column collapse.

portional to a modified particle Reynolds number Re_p (Meruane et al., 2010) defined as:

$$\frac{f_2}{f_1} \approx Re_p = \frac{D\rho_L||\mathbf{v}_L - \mathbf{v}_S||}{v_m} \tag{12}$$

For low Re_p, the quadratic term f_2 is negligible compared to the linear term f_1. In the following, the reference velocity for the solid phase is assumed $v_{S,ref} = \sqrt{gH_0}$, which is a reasonable reference value for the solid front velocity as shown in Jing et al. (2018). The reference velocity for the liquid phase is assumed $v_{L,ref} = \sqrt{gH_0}$, which is the free fall velocity. Note that $v_{L,ref} - v_{S,ref}$ does not represent any true relative velocity between phases during the collapse, but it is considered as a representative parameter of the solid–fluid interaction.

In order to explore the importance of the quadratic term in Eq. (7) we performed parametric analyses increasing the size of the column up to a factor of 100 while keeping $a = 1.5$. The liquid viscosity v_m is varied between $0.001\ \mathrm{Pa \cdot s}$ and $0.1\ \mathrm{Pa \cdot s}$ and the grain size D between 0.0025 m and 0.25 m while keeping $\rho_L = 1000\ \mathrm{kg/m^3}$ and $\rho_S = 2600\ \mathrm{kg/m^3}$. Only MPM simulations are performed in this case due to the high computational cost requested to perform similar DEM-LBM simulations.

Fig. 13 illustrates the results for two different values of the particle Reynolds number $Re_p = 4 \cdot 10^3$ and $Re_p = 4 \cdot 10^5$, showing the position of LMPs and SMPs at different time instants. The results obtained using the linear and the quadratic term in Eq. (7) are shown in panels (*a-f*). Those obtained using only the linear term are shown in panels (*g-l*).

In the case $Re_p = 4 \cdot 10^3$, shown in Fig. 13 (*a-c*,*g-i*), there is no clear separation between fluid and solid fronts. Neglecting the quadratic term of the drag force does not significantly alter the results. In contrast, for $Re_p = 4 \cdot 10^5$, Fig. 13 (*d-f*,*j-l*), the fluid can easily flow out of the mixture, and in this case the effect of the quadratic term is significant.

The results of the parametric analyses showed that the importance of term f_2 in Eq. (7) becomes significant for the relative position between fluid and solid front approximately for $Re_p > 4 \cdot 10^4$. This means that an appropriate formulation of the drag force is crucial to capture correctly the solid–fluid interaction in these phenomena, especially for high Reynolds numbers.

6. Conclusions

This paper discusses the numerical simulation of a saturated granular column collapse in air. The benchmark case is provided by an experimental campaign performed on a small-scale physical model. We present and compare two numerical methods: DEM-LBM and 2D-DP MPM, respectively discrete- and continuum-based. Both are multiphase, and can simulate solid–fluid interactions in granular materials, including separations between the constituents.

DEM-LBM applies a micromechanical approach to simulate grain-grain interactions, at the cost of requiring a very fine discretization for the fluid phase. While the discrete approach offers more insight into the microscopic structure of the granular material, it is also computationally demanding, with the algorithm cost growing with the total number of particles and with the decrease of the mesh size (Δ). This limits the simulations to relatively large grains, or small samples. On the other hand, the efficiency of MPM is not altered by the grain size, making it easily applicable to real-scale problems.

The 2D-DP MPM model predicts a faster collapse with higher velocities compared to DEM-LBM. We believe this is mainly due to the constitutive model (Mohr–Coulomb). Additionally, in saturated conditions DEM-LBM can account for negative excess pore pressure, thus reducing granular mobility, especially when significant dilating volumetric deformations are expected. In any case, the runout is similar and in relatively good agreement with the experimental results. This is probably due to the physical model featuring grains arranged in a loose packing, and thus limiting the effect of dilation.

The pure-continuum assumptions of 2P-DP MPM arise questions on the modelling of the drag force, on the fluidization process, and on the constitutive model of the constituents. In particular, the drag force expressed in Eq. (6) produces realistic results, especially in terms of runout. It also seems to be appropriate in a wide range of cases. The effect of the quadratic term in the formulation appears negligible for small values of the particle Reynolds number as defined as in Section 5.3. The parametric analysis showed

Please cite this article as: F. Ceccato, A. Leonardi, V. Girardi et al., Numerical and experimental investigation of saturated granular column collapse in air, Soils and Foundations, https://doi.org/10.1016/j.sandf.2020.04.004

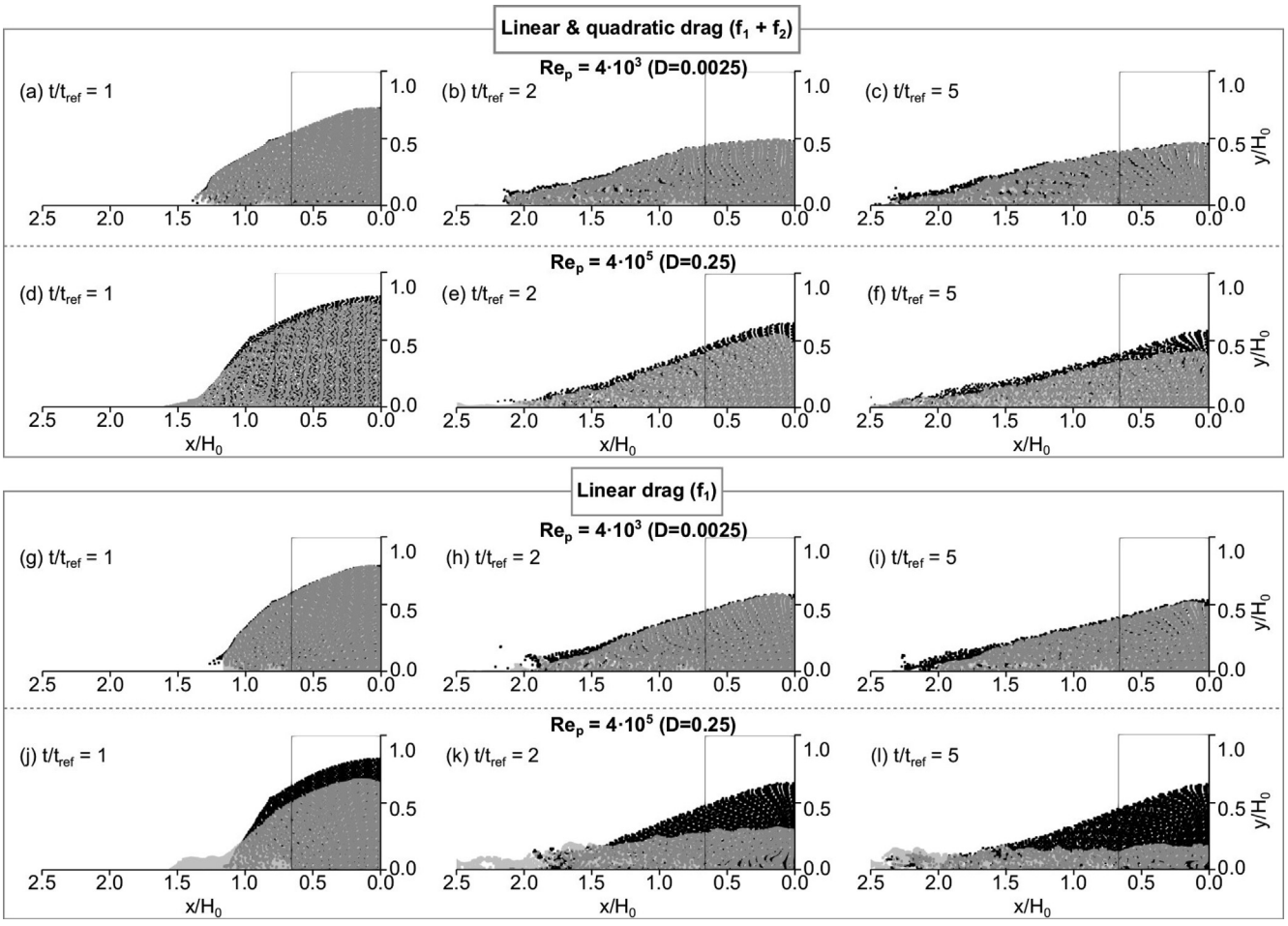

Fig. 13. MPM simulations: Position of LMPs (grey) and SMPs (black) at different time instants using linear and quadratic terms in Eq. (7) (*a-f*) or only linear term (*g-i*). Comparisons for $Re_p = 4 \cdot 10^3$ (*a-c*) and (*g-i*) and $Re_p = 4 \cdot 10^5$ (*d-f*) and (*.j-l*).

that the importance of this term is negligible for $Re_p < 10^4$. However, the wide variability of conditions under which saturated granular material can be encountered clearly requires these aspects to be further investigated in the future.

Currently, simple elasto-plastic models are used for the solid and the criteria of maximum porosity is applied for the solid–fluid transition with reasonably good results. Recently, constitutive models incorporating Kinetic theory and critical state soil mechanics have been proposed for dry granular flows at different shear rates (Redaelli et al., 2015; Redaelli et al., 2017a; Redaelli et al., 2017b), but the extension to saturated conditions is still in progress (Redaelli et al., 2019). LBM-DEM can be effectively used to develop and validate these types of constitutive models. Further, it can support their implementation in MPM or other continuum-based models, and their application to benchmark examples such as the one presented in this paper.

Acknowledgements

The authors acknowledge the support of Domino Project from the Water JPI, the WaterWorks2014 Cofunded Call, the European Commission (Horizon 2020), and the Italian Ministry of Education, University and Research (MIUR). Computational resources for the DEM-LBM simulations were provided by HPC@POLITO, a project of Academic Computing within the Department of Control and Computer Engineering at Politecnico di Torino (www.hpc.polito.it).

References

Abe, K., Soga, K., Bandara, S., 2013. Material point method for coupled hydromechanical problems. J. Geotech. Geoenviron. Eng. 140, 1–16. https://doi.org/10.1061/(ASCE)GT.1943-5606.0001011.

Artoni, R., Santomaso, A.C., Gabrieli, F., Tono, D., Cola, S., 2013. Collapse of quasi-two-dimensional wet granular columns. Phys. Rev. E – Stat. Nonlinear Soft Matter Phys. 87, 1–8. https://doi.org/10.1103/PhysRevE.87.032205, arXiv:1401.2028.

Bandara, S., Soga, K., 2015. Coupling of soil deformation and pore fluid flow using material point method. Comput. Geotech. 63, 199–214. https://doi.org/10.1016/j.compgeo.2014.09.009.

Beenakker, C., 1984. The effective viscosity of a concentrated suspension of spheres (and its relation to diffusion). Physica A 128, 48–81.

Bougouin, A., Lacaze, L., 2018. Granular collapse in a fluid: Different flow regimes for an initially dense-packing. Phys. Rev. Fluids 064305, 1–23. https://doi.org/10.1103/PhysRevFluids.3.064305.

Brezzi, L., 2018. Collapse of granular – cohesive soil mixtures on a horizontal plane. Acta Geotech. 7. https://doi.org/10.1007/s11440-018-0725-7.

Ceccato, F., Simonini, P., 2016. Granular flow impact forces on protection structures: MPM numerical simulations with different constitutive models. Procedia Eng. 158, 164–169. https://doi.org/10.1016/j.proeng.2016.08.423.

Ceccato, F., Simonini, P., 2019. Numerical features used in simulations. In: Fern, J., Rohe, A., Soga, K., Alonso, E. (Eds.), The Material Point Method for Geotechnical Engineering. CRC Press. chapter 6, pp. 101–124. doi:10.1201/9780429028090-6.

Crosta, G.B., Imposimato, S., Roddeman, D.G., 2003. Numerical modelling of large landslides stability and runout. Natural Hazards Earth Syst. Sci. 3, 523–538. https://doi.org/10.5194/nhess-3-523-2003.

Dai, Z., Huang, Y., Cheng, H., Xu, Q., 2017. SPH model for fluid–structure interaction and its application to debris flow impact estimation. Landslides 14, 917–928. https://doi.org/10.1007/s10346-016-0777-4.

Delannay, R., Valance, A., Mangeney, A., Roche, O., Richard, P., 2017. Granular and particle-laden flows: From laboratory experiments to field observations. J. Phys. D: Appl. Phys. 50. https://doi.org/10.1088/1361-6463/50/5/053001.

Ergun, S., 1952. Fluid flow through packed column. Chem. Eng. Prog.

Feng, Y.T., Han, K., Owen, D.R.J., 2010. Combined three-dimensional lattice Boltzmann method and discrete element method for modelling fluid – particle interactions with experimental assessment. Int. J. Numer. Meth. Eng. 81, 229–245. https://doi.org/10.1002/nme.

Fern, E.J., Soga, K., 2016. The role of constitutive models in MPM simulations of granular column collapses. Acta Geotech. 11, 659–678. https://doi.org/10.1007/s11440-016-0436-x.

Fern, J., Rohe, A., Soga, K., Alonso, E., 2019. The Material Point Method for Geotechnical Engineering: A Practical Guide. CRC Press.

Forchheimer, P., 1901. Wasserbewegung durch Boden. Zeitschrift des Vereins Deutscher Ingenieure.

Hill, K., Tan, D., 2014. Segregation in dense sheared flows: gravity, temperature gradients, and stress partitioning. J. Fluid Mech. 756, 54–88. https://doi.org/10.1017/jfm.2014.271.

Hungr, O., Leroueil, S., Picarelli, L., 2014. The Varnes classification of landslide types, an update. Landslides 11, 167–194. https://doi.org/10.1007/s10346-013-0436-y.

Janßen, C., Krafczyk, M., 2011. Free surface flow simulations on GPGPUs using the LBM. Comput. Math. Appl. 61, 3549–3563. https://doi.org/10.1016/j.camwa.2011.03.016.

Jing, L., Yang, G.C., Kwok, C.Y., Sobral, Y.D., 2018. Dynamics and scaling laws of underwater granular collapse with varying aspect ratios. Phys. Rev. E 98, 1–15. https://doi.org/10.1103/PhysRevE.98.042901.

Kumar, K., Delenne, J.Y., Soga, K., 2017. Mechanics of granular column collapse in fluid at varying slope angles. J. Hydrodyn. 29, 529–541. https://doi.org/10.1016/S1001-6058(16)60766-7.

Lagrée, P.Y., Staron, L., Popinet, S., 2011. The granular column collapse as a continuum: validity of a two-dimensional Navier-Stokes model with a mu(I)-rheology. J. Fluid Mech. 686, 378–408. https://doi.org/10.1017/jfm.2011.335.

Leonardi, A., Cabrera, M., Wittel, F.K., Kaitna, R., Mendoza, M., Wu, W., Herrmann, H.J., 2015a. Granular-front formation in free-surface flow of concentrated suspensions. Phys. Rev. E – Stat. Nonlinear Soft Matter Phys. 92, 052204. https://doi.org/10.1103/PhysRevE.92.052204.

Leonardi, A., Pokrajac, D., Roman, F., Zanello, F., Armenio, V., 2018. Surface and subsurface contributions to the build-up of forces on bed particles. J. Fluid Mech. 851, 558–572. https://doi.org/10.1017/jfm.2018.522.

Leonardi, A., Wittel, F.K., Mendoza, M., Herrmann, H.J., 2015b. Lattice-Boltzmann method for geophysical plastic flows. In: Wu, W. (Ed.), Recent Advances in Modeling Landslides and Debris Flows. Springer International Publishing, Cham. Springer Series in Geomechanics and Geoengineering, pp. 131–140. doi:10.1007/978-3-319-11053-0.

Li, D., Engler, T.W., et al., 2001. Literature review on correlations of the non-darcy coefficient. In: SPE Permian Basin Oil and Gas Recovery Conference, Society of Petroleum Engineers.

Li, X., Zhao, J., 2018. Dam-break of mixtures consisting of non-Newtonian liquids and granular particles. Powder Technol. 338, 493–505. https://doi.org/10.1016/j.powtec.2018.07.021.

Lube, G., Huppert, H.E., Sparks, R.S.J., Freundt, A., 2005. Collapses of two-dimensional granular columns. Phys. Rev. E – Stat. Nonlinear Soft Matter Phys. 72, 1–10. https://doi.org/10.1103/PhysRevE.72.041301.

Marchelli, M., Leonardi, A., Pirulli, M., Scavia, C., 2019. On the efficiency of slit dams in retaining granular flows. Géotechnique, in press. doi:10.1680/jgeot.18.p.044.

Martinelli, M., 2016. Soil-water interaction with Material Point Method. Double-Point Formulation. Technical Report. Report on EU-FP7 research project MPM-Dredge PIAP-GA-2012-324522.

Martinelli, M., Rohe, A., 2015. Modelling fluidisation and sedimentation using material point method. In: Idelsohn, S., Sonzogni, V., Coutinho, A., Cruchaga, M., Lew, A., Cerrolaza, M. (Eds.), Proc. 1st Pan-American Congress on Computational Mechanics (PANACM 2015), Buenos Aires, Argentinia. doi:10.13140/RG.2.1.4638.3445.

Mast, C.M., Arduino, P., Mackenzie-Helnwein, P., Miller, G.R., 2014. Simulating granular column collapse using the Material Point Method. Acta Geotech. 10, 101–116. https://doi.org/10.1007/s11440-014-0309-0.

Meruane, C., Tamburrino, A., Roche, O., 2010. On the role of the ambient fluid on gravitational granular flow dynamics. J. Fluid Mech. 648, 381–404. https://doi.org/10.1017/S0022112009993181.

Orodu, O.D., Makinde, F.A., Orodu, K.B., 2012. Experimental study of darcy and non-darcy flow in porous media. Int. J. Eng. Technol. 2, 1934–1943.

Pirulli, M., Bristeau, M.O., Mangeney, A., Scavia, C., 2007. The effect of the earth pressure coefficients on the runout of granular material. Environ. Modell. Softw. 22, 1437–1454. https://doi.org/10.1016/j.envsoft.2006.06.006.

Redaelli, I., Ceccato, F., Di Prisco, C., Simonini, P., 2017a. Solid-fluid transition in granular flows: MPM simulations with a new constitutive approach. Procedia Eng. 175, 80–85. https://doi.org/10.1016/j.proeng.2017.01.028.

Redaelli, I., Ceccato, F., Prisco, C., Simonini, P., 2017b. MPM simulations of granular column collapse with a new constitutive model for the solid-fluid transition. In: 5th International Conference on Particle-Based Methods – Fundamentals and Applications, PARTICLES 2017, pp. 539–545.

Redaelli, I., Marveggio, P., Prisco, C.D., 2019. Constitutive modelling of phase transition in granular materials. In: 2nd International Conference on the Material Point Method for Modelling Soil-Water-Structure Interaction, Cambridge.

Redaelli, I., di Prisco, C., Vescovi, D., 2015. A visco-elasto-plastic model for granular materials under simple shear conditions. Int. J. Numer. Anal. Meth. Geomech., n/a–n/adoi:10.1002/nag.2391.

Roux, J.N., Combe, G., 2002. Quasistatic rheology and the origins of strain. C.R. Phys. 3, 131–140. https://doi.org/10.1016/S1631-0705(02)01306-3.

Santomaso, A.C., Volpato, S., Gabrieli, F., 2018. Collapse and runout of granular columns in pendular state. Phys. Fluids 30. https://doi.org/10.1063/1.5030779.

Solowski, W., Sloan, S., 2013. Modelling of sand column collapse with material point method. In: Proceedings of the 3rd International Symposium on Computational Geomechanics (ComGeo III).

Steffen, M., Kirby, R., Berzins, M., 2010. Decoupling and balancing of space and time errors in the material point method (MPM). Int. J. Numer. Meth. Eng. 82, 1207–1243. https://doi.org/10.1002/nme.

Sun, W.C., Kuhn, M.R., Rudnicki, J.W., 2013. A multiscale DEM-LBM analysis on permeability evolutions inside a dilatant shear band. Acta Geotech. 8, 465–480. https://doi.org/10.1007/s11440-013-0210-2.

Švec, O., Skoček, J., Stang, H., Geiker, M.R., Roussel, N., 2012. Free surface flow of a suspension of rigid particles in a non-Newtonian

fluid: A lattice Boltzmann approach. J. Nonnewton. Fluid Mech. 179–180, 32–42. https://doi.org/10.1016/j.jnnfm.2012.05.005.

Vardoulakis, I., 2004. Fluidisation in artesian flow conditions: Hydromechanically stable granular media. Géotechnique 54, 117–130. https://doi.org/10.1680/geot.2004.54.2.117.

Xiong, Q., Madadi-Kandjani, E., Lorenzini, G., 2014. A LBM–DEM solver for fast discrete particle simulation of particle–fluid flows. Continuum Mech. Thermodyn. 26, 907–917. https://doi.org/10.1007/s00161-014-0351-z.

Yang, G.C., Jing, L., Kwok, C.Y., Sobral, Y.D., Engineering, C., Building, H.W., Road, P., Kong, H., 2019. A comprehensive parametric study of LBM-DEM for immersed granular flows. Comput. Geotech. 114, 103100. https://doi.org/10.1016/j.compgeo.2019.103100.

Zhang, X., Krabbenhoft, K., Sheng, D., Li, W., 2015. Numerical simulation of a flow-like landslide using the particle finite element method. Comput. Mech. 55, 167–177. https://doi.org/10.1007/s00466-014-1088-z.

Zhao, X., Liang, D., Martinelli, M., 2017. Numerical simulations of dam-break floods with mpm. Procedia Eng. 175, 133–140.

Please cite this article as: F. Ceccato, A. Leonardi, V. Girardi et al., Numerical and experimental investigation of saturated granular column collapse in air, Soils and Foundations, https://doi.org/10.1016/j.sandf.2020.04.004